

Multi-band superconductivity and nanoscale inhomogeneity at oxide interfaces

S. Caprara^{1,2}, J. Biscaras³, N. Bergeal³, D. Bucheli¹, S. Hurand³, C.

Feuillet-Palma³, A. Rastogi⁴, R. C. Budhani^{4,5}, J. Lesueur³, and M. Grilli^{1,2}

¹*Dipartimento di Fisica, Università di Roma “La Sapienza”, Piazzale Aldo Moro 5, 00185 Roma, Italy*

²*ISC-CNR and Consorzio Nazionale Interuniversitario per le Scienze Fisiche della Materia, Unità di Roma “Sapienza”*

³*LPEM-UMR8213/CNRS-ESPCI Paris Tech - UPMC, 10 rue Vauquelin - 75005 Paris, France*

⁴*Condensed Matter - Low Dimensional Systems Laboratory, Department of Physics,
Indian Institute of Technology Kanpur, Kanpur 208016, India*

⁵*National Physical Laboratory, New Delhi - 110012, India*

(Dated: March 2, 2022)

The two-dimensional electron gas at the $\text{LaTiO}_3/\text{SrTiO}_3$ or $\text{LaAlO}_3/\text{SrTiO}_3$ oxide interfaces becomes superconducting when the carrier density is tuned by gating. The measured resistance and superfluid density reveal an inhomogeneous superconductivity resulting from percolation of filamentary structures of superconducting “puddles” with randomly distributed critical temperatures, embedded in a non-superconducting matrix. Following the evidence that superconductivity is related to the appearance of high-mobility carriers, we model intra-puddle superconductivity by a multi-band system within a weak coupling BCS scheme. The microscopic parameters, extracted by fitting the transport data with a percolative model, yield a consistent description of the dependence of the average intra-puddle critical temperature and superfluid density on the carrier density.

PACS numbers: 74.81.-g,73.20.-r,73.40.-c,74.20.-z

The discovery of superconductivity in the two-dimensional electron gas (2DEG) formed at certain oxide interfaces such as $\text{LaAlO}_3/\text{SrTiO}_3$ (LAO/STO) or $\text{LaTiO}_3/\text{SrTiO}_3$ (LTO/STO) [1–4] has attracted great interest and stimulated intense research activity. The possibility of tuning the carrier density by means of electrostatic gating in these extremely two-dimensional superconductors (the Fermi wavelength being smaller than the thickness of the gas[4]) opens new opportunities to study fundamental issues in quantum fluids[5]. More generally, these 2DEG appear as very rich quantum matter systems, since they also present magnetism [6–9] and strong tunable spin-orbit coupling [10, 11]. As for every two dimensional systems, disorder is expected to play a relevant role on their physical properties. Recent magnetotransport measurements revealed the existence of two kinds of carriers in LTO/STO, with high and low mobility respectively[4]. It has been suggested that superconductivity is related to the appearance of the high-mobility carriers[4, 12] with an inhomogeneous character, i.e. superconducting “puddles” embedded in a (weakly localizing) metallic background[5]. Direct superfluid density[9] and magnetic[8] measurements display signs of strong inhomogeneity at micrometric scales. Recent current distribution[13] and surface potential studies[14] reveal stripes structures in these interfaces. Given all these signs of inhomogeneities, one has first to analyze the role of disorder before getting further insight in the physics of the 2DEG, and for example, explain the rapid decrease of T_c with the gate voltage while under-doping.

Our aim is on the one hand to infer a more detailed structure of the inhomogeneous state and on the other hand to provide a description for superconductivity in an inhomogeneous system with different kinds of carriers. We first show that resistance measurements[4] and the topographic mapping of the superfluid density on micrometric scale[9] can be phenomenologically accounted for within a scheme of a percolative inhomogeneous 2DEG with poor long-distance connectivity, but substantial superconducting (SC) current loops to warrant a high fraction of diamagnetic response. We then show that the properties of the SC puddles (e.g., their fraction, and critical temperatures) can be extracted from experiments and used at a microscopic level to model the intra-puddle multi-carrier pairing, gaining insight about the pairing mechanism. Although some features of the diamagnetic response are seemingly related to a strong coupling SC behavior[9], our analysis demonstrates that inhomogeneities and multi-band superconductivity fully account for the SC behavior of these systems within a standard weak coupling BCS scheme.

— *Sheet resistance* — We have recently shown that the percolative SC transition in inhomogeneous systems, like the oxide interfaces, is well described by the Effective Medium Theory (EMT) [15]. For samples exhibiting a resistance drop due to superconductivity, the measured sheet resistance of LTO/STO is well fitted by the EMT with a SC fraction $w < 1$ (the SC puddles). Each puddle has a random local critical temperature T_c , which we assume to have a Gaussian distribution, with mean \bar{T}_c and width γ . The weight w of the T_c distribution represents the fraction of SC puddles and the non SC fraction $1 - w$ represents the metallic background (we refer the reader to Ref. [15] for details). The sheet resistance at any temperature is

$$R(T) = R^\infty \left[w \operatorname{erf} \left(\frac{T - \bar{T}_c}{\sqrt{2}\gamma} \right) + 1 - w \right],$$

with fitting parameters R^∞ (high-temperature sheet resistance), w , \bar{T}_c , and γ . The percolative SC transition, marked by a vanishing R , takes place at a temperature $T_p \leq \bar{T}_c$, such that

$$\operatorname{erf} \left(\frac{T_p - \bar{T}_c}{\sqrt{2}\gamma} \right) = 1 - \frac{1}{w}. \quad (1)$$

This equation has a solution for T_p only if $w \geq \frac{1}{2}$, i.e., if the SC fraction can percolate in the two-dimensional system. When T_p becomes negative or is not defined, the system remains resistive down to $T = 0$, although a significant reduction of sheet resistance may still occur, witnessing the presence of a sizable (though not percolating) SC fraction.

Fig. 1 (a) reports the measured sheet resistance as a function of temperature for various values of the gate voltage V_g in a LTO/STO sample, and the fitting EMT curves. From the fits one can extract the average intra-puddle critical temperature \bar{T}_c [corresponding to the temperature of maximal slope of $R(T)$ within EMT], which is reported in Fig. 3 (a) as a function of V_g (red solid line and empty circles). The fits also provide the fraction of SC regions w [displayed in Fig. 1 (c) as a function of V_g]. Since EMT disregards spatial correlations, the simultaneous request of a percolating SC cluster and the tailish shape of the resistance near percolation force the weight of the regions which can become SC to be $w \approx \frac{1}{2}$ [15] (Fig. 1(c), see also Supplemental Material). Fig. 1(d) reports the width γ of the Gaussian distribution of T_c , which diverges as the fraction w of the SC puddles goes to zero. This is rather natural because the density decrease emphasizes the effects of disorder so that fluctuations of the local superconductivity increase, leading to a substantial broadening of the T_c distribution. We will show later a more precise description of this phenomenon within the two-bands model.

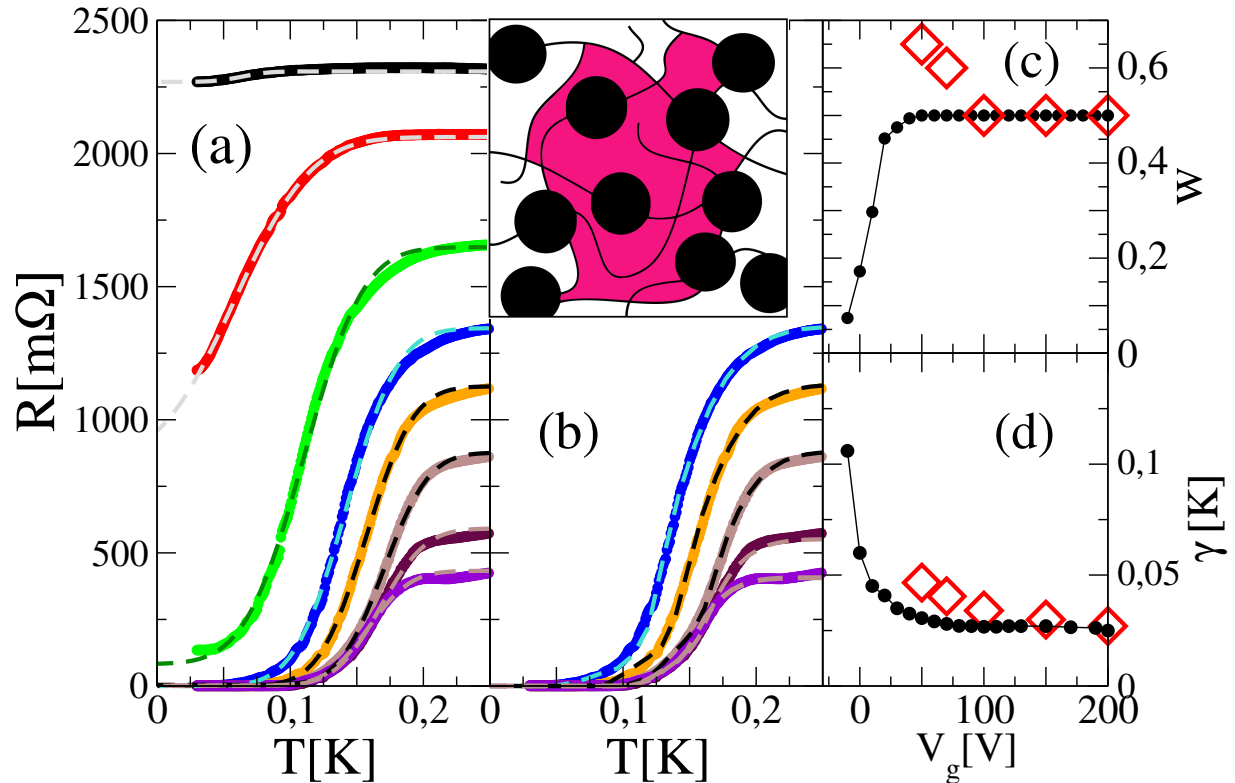


FIG. 1. (a) Sheet resistance as a function of temperature in a LTO/STO sample for various values of the gate voltage. From top to bottom $V_g = -10, 10, 30, 50, 70, 100, 150, 200$ V. Symbols mark the experimental data, while the dashed lines are the theoretical fits using the EMT (see text). (b) From top to bottom $V_g = 50, 70, 100, 150, 200$ V. Symbols mark the experimental data, while the dashed lines are the theoretical fits using the RRN (see text). Inset: sketch of an inhomogeneous RRN system with a SC filamentary+baubles cluster. The shaded region is a closed loop contributing to the diamagnetic response. (c) SC fraction w extracted from the fits of the sheet resistance within EMT (filled circles, solid line) and within the RRN (empty diamonds). (d) Width of the Gaussian distribution of T_c used in the fits of the sheet resistance within the EMT (filled circles, solid line) and within the RRN (empty diamonds).

— *Superfluid density* — The superfluid density was measured in LAO/STO interfaces using a scanning SQUID probe averaging over micrometric regions [9]. This technique is not sensitive to submicrometric inhomogeneities, but revealed a *distribution* of superfluid densities within a given sample on the micrometric scale, thereby supporting the idea of inhomogeneous 2DEG at these oxide interfaces. Since the sheet resistance curves of these systems are similar to those of LTO/STO interfaces, we assume that our percolative EMT analysis also applies in this case and that the measured local superfluid density is an average over an inhomogeneous state of submicrometric puddles [17].

To capture this effect, we extend the EMT to small but finite frequency ω . We model the metallic regions with a Drude-like complex conductivity $\sigma_N(\omega) = B/(A + i\omega)$ and the SC regions with a purely reactive conductivity $\sigma_S(\omega) = B/(i\omega)$. We introduce the quantities $\rho_S(\omega) = 1/\sigma_S(\omega) = i\omega/B$ and $\rho_N(\omega) = 1/\sigma_N(\omega) = \rho_0 + \rho_S(\omega)$, with $\rho_0 = A/B$. At high temperature, the system is metallic and $\rho(\omega) = 1/\sigma(\omega) = \rho_N$ everywhere. However, within the SC puddles, ρ_0 vanishes as soon as the local critical temperature is reached. The solution of the EMT equation, neglecting higher frequency terms $\sim \omega^2$, is

$$\rho(\omega) \approx \rho_0(w_N - w_S)\vartheta(w_N - w_S) + \frac{\rho_S(\omega)}{|w_N - w_S|},$$

where $\vartheta(x)$ is the Heaviside step function, w_S is the fraction of puddles that have become SC (at a given temperature T), and $w_N = 1 - w_S$ is the metallic fraction (resulting both from puddles that have not yet become SC and from the

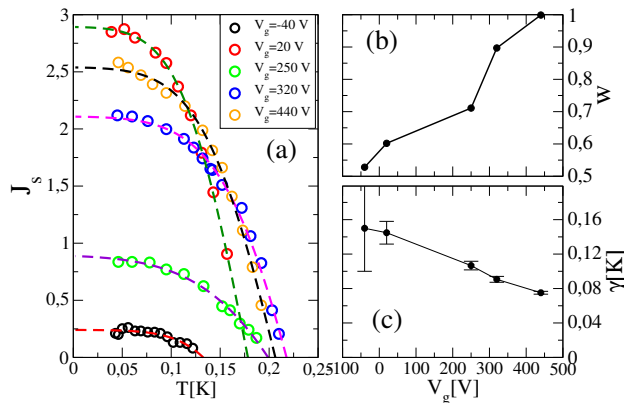


FIG. 2. (a) EMT fits of the superfluid density in LAO/STO (lines) as a function of temperature for various gate voltages. The experimental data (symbols) are extracted from Ref. 9. (b) SC fraction w responsible for the diamagnetic response. (c) Width of the Gaussian distribution of T_c used in the fits of the superfluid density.

metallic background). Evidently, when $w_N > w_S$, the system displays a Drude-like complex conductivity. However, below the percolation temperature T_p (if any), $w_S > w_N$, and we find a purely reactive conductivity

$$\sigma(\omega) = \frac{1}{\rho(\omega)} = \frac{A(w_S - w_N)}{i\omega}.$$

Therefore, for $T < T_p$ and w given by Eq.(1), the superfluid density of the percolating network is

$$\begin{aligned} J_s &\propto w_S - w_N = w - 1 - w \operatorname{erf} \left(\frac{T - \bar{T}_c}{\sqrt{2}\gamma} \right) \\ &= w \left[\operatorname{erf} \left(\frac{T_p - \bar{T}_c}{\sqrt{2}\gamma} \right) - \operatorname{erf} \left(\frac{T - \bar{T}_c}{\sqrt{2}\gamma} \right) \right]. \end{aligned} \quad (2)$$

Fig. 2 (a) reports this micrometrically averaged superfluid density together with our EMT fits [Eq. (2)] at various gate voltages V_g . Remarkably, the T dependence of $J_s(T)/J_s(T=0)$ mimics the qualitative behavior of the BCS prediction, but may quantitatively deviate from it. The slope at the transition, for instance, is ruled by the width γ of the distribution of critical temperatures. We can thus account for the deviations from standard BCS observed in Ref. 9, which were attributed to a tendency to strong coupling. Our alternative explanation for these deviations is that the system is in a weak coupling regime, but the percolative superfluid density is ruled by the submicrometric distribution of inhomogeneities averaged at the micron scale by the SQUID pick-up loop used in Ref 9. The fits allow to obtain the fraction w of SC puddles extracted from diamagnetic measurements which is reported in Fig. 2(b). It ranges from 1/2 to 1, and is therefore always larger than the fraction obtained from transport measurements. This is fully consistent within a percolative description of the system: resistance measurements mainly probe the direct percolative path, regardless of dead-ends and disconnected SC regions[16], while screening measurements are sensitive to all SC loops, even when not connected to the backbone. In this case, the diamagnetic fraction can be nearly one, while the connectivity for macroscopic transport can be very small (or even vanishing) if many SC puddles or loops are disconnected [see the sketch in the inset of Fig. 1(b)]. Fig. 2(c) displays the behavior of the width γ of the T_c distribution. Despite the differences in material and physical quantities, γ has a similar behavior to the γ from transport in LTO/STO [Fig. 1(d)] and is of comparable magnitude.

— *Effect of space correlations* — The explanation of the above discrepancy between the SC weight w in transport and magnetic experiments rests on the filamentary structure of the SC fraction in LXO/STO systems, which is one of the two main outcomes of our work. However, the above results (and fits) have been obtained within the EMT, which is a mean-field-like approach neglecting space correlations. Therefore, to substantiate the above interpretation, it is important to test how robust is the finding that the SC fraction involved in transport is rather small, $w \approx 0.5$, within a model, which takes into account the space correlations inherent in the filamentary structure. To this purpose, we refine our model and solve a random resistor network (RRN) where the SC regions only occur on a cluster with strong space correlations embedded in a metallic matrix. Based on a preliminary analysis [18], showing that the tailish sheet resistance implies both a dense SC cluster at short distances and a filamentary structure at larger distance, we numerically generate a fractal-like structure[18, 19]. Due to the poor long-distance connectivity,

percolation only occurs when the resistance of almost all bonds has been switched off. For a Gaussian distribution of critical temperatures, the system is thus forced to explore the low temperature asymptotic of the distribution, thereby producing a tailish resistance[20]. On the other hand, a purely filamentary structure, although dense at short distance due to the almost fractal cluster, is still too faint ($w \lesssim 0.3$) and fails to reproduce accurately the high temperature part of the $R(T)$ curves. Thus in order to vary the density of the SC cluster without crucially changing the long-range connectivity, we decorate the filaments with randomly distributed circular “superpuddles”, their number being chosen to yield RRNs with weights w ranging from 0.3 to 0.7 (see Supplemental Material). The resulting clusters look like a filamentary “Christmas tree” with decorating baubles [see inset of Fig. 1 (b)]. Fig. 1 (b) reports fits of the sheet resistance using resistivity curves calculated on such Christmas trees. Noticeably, even though the SC weight w is not forced to $\frac{1}{2}$ like in EMT, we still find that the sheet resistance only acquires a tailish behavior if $0.5 \lesssim w \lesssim 0.65$ (Fig. 1 (c)), where the lower bound is imposed by the high slope at intermediate temperatures and the upper bound is due to the tailish behavior close to percolation. Fig. 1 (d) reports the width γ of the Gaussian distribution of T_c obtained within the Christmas tree model. One can see that γ follows the same qualitative behavior as in the EMT case with a substantial increase upon lowering the voltage. As a conclusion, EMT and RRN models lead to very close results about the T_c distribution and its variation with the gate voltage provided a filamentary Christmas tree structure is used for the RRN.

— *Multiband BCS scenario* — The inhomogeneous character of LXO/STO systems, clearly apparent both in the normal-state [$R(T)$] and in the SC [$J_s(T)$] properties, entails a distribution of local critical temperatures with an average depending on the overall density (i.e., gating) $\bar{T}_c(V_g)$. This dependence can be extracted from the resistance fits [Fig. 3] and it provides insight on the intra-puddle pairing mechanism. A recent magnetotransport analysis [4] demonstrated the coexistence of a rather large density of low-mobility carriers with a smaller density of high-mobility carriers in the SC regime of LTO/STO. In particular, superconductivity seems to be triggered by the presence of the high-mobility carriers. A similar behavior seems to occur in LAO/STO [21]. According to this scenario, we propose that the 2DEG formed at the LXO/STO interface may be described as a multi-band system [22–25], and the occurrence of superconductivity may be captured by means of a BCS-like Hamiltonian (see Supplemental Material). We take for the ℓ -th sub-band of our 2DEG a parabolic dispersion law

$$\varepsilon_{\mathbf{k},\ell} = \bar{\varepsilon}_\ell + \frac{\hbar^2 k_x^2}{2m_{\ell,x}} + \frac{\hbar^2 k_y^2}{2m_{\ell,y}},$$

where m is the (possibly anisotropic) effective mass of the charge carriers. Following the evidence that superconductivity is related to the appearance of high-mobility carriers, we represent the whole set of low-lying bands with one sub-band ($\ell = 1$) collecting all the low-mobility carriers with vanishingly small T_c , while the high-mobility carriers in the sub-band $\ell = 2$ give rise to a finite T_c . Thus, SC puddles are regions where the sub-band $\ell = 2$ is locally filled, whereas the (weakly localizing) metallic background corresponds to regions where the sub-band $\ell = 2$ is empty. To reproduce the experimental results, we are led to a suitable choice of the pairing amplitudes $g_{\ell\ell'}$ (intra-band for $\ell = \ell'$, interband, for $\ell \neq \ell'$): $g_{11} \ll (g_{12}, g_{21}) \ll g_{22}$ (this condition is consistent with the analysis of a two-band model in Ref. 26). According to the standard BCS approach, the pairing amplitudes are only effective in a limited dynamical range $|\varepsilon_{\mathbf{k},\ell} - \mu|, |\varepsilon_{\mathbf{k},\ell'} - \mu| \leq \hbar\omega_0$, where ω_0 is a characteristic frequency of the mode that mediates pairing and μ is the chemical potential. We assume henceforth that the bottoms of the two sub-bands are well separated, $\bar{\varepsilon}_2 - \bar{\varepsilon}_1 \gg \hbar\omega_0$, and take $\bar{\varepsilon}_2 = 0$ as the reference energy level.

While more general (though standard) expressions are derived in the Supplemental Material, here we only report the expressions obtained for $g_{11} = g_{12} = g_{21} = 0$, so that the system is not SC until the carrier density reaches the value such that $\mu = 0$. For $0 < \mu < \hbar\omega_0$, T_c increases with increasing μ

$$T_c \approx 1.14 \sqrt{\hbar\omega_0 \mu} e^{-1/\lambda_2},$$

where we merged into the single dimensionless coupling $\lambda_2 \equiv N_2^0 g_{22}$ the intraband g_{22} coupling and the density of states N_2^0 of the $\ell = 2$ sub-band. For $\mu > \hbar\omega_0$, T_c saturates to its maximum (BCS) value $T_c^{max} \approx 1.14 \hbar\omega_0 e^{-1/\lambda_2}$. Thus, $T_c(\mu) = 0$, for $\mu < 0$, $T_c(\mu) = T_c^{max} \sqrt{\mu/\hbar\omega_0}$, for $0 \leq \mu \leq \hbar\omega_0$, $T_c(\mu) = T_c^{max}$, for $\mu \geq \hbar\omega_0$, and the range of variation of μ which corresponds to an increasing T_c is a direct measure of the characteristic energy scale of the pairing mediator, $\hbar\omega_0$.

We now proceed to fit the curve $\bar{T}_c(V_g)$ extracted from the experimental data by means of EMT, with our theoretical curve $T_c(\mu)$. The relation between V_g and μ is only approximately linear and its determination is described in detail in the Supplemental Material. The resulting critical temperature for various values of V_g is reported in Fig. 3 (blue dashed line and crosses). From the fit, we finally obtain the dimensionless coupling constant $\lambda_2 \approx 0.25$ (which, consistently with our assumption, is in the weak coupling regime) and $\hbar\omega_0 \approx 23$ meV, which is the energy typical of phonons in STO[27].

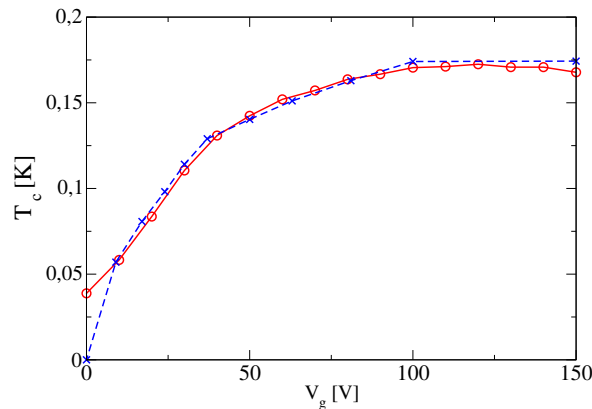


FIG. 3. \bar{T}_c extracted from the EMT fit to experimental data (red solid line and empty circles) and the theoretical T_c calculated within the two band model (see text), as a function of the gate voltage V_g (blue dashed line and crosses).

In conclusion, we describe the superconductivity in LAO/STO and LTO/STO oxide interfaces within a scenario in which SC puddles form a percolating network. In this framework we showed here that the sheet resistance in LTO/STO interfaces is very well described by EMT or by a Christmas tree model of RRN for an inhomogeneous 2DEG with a substantial filamentary character. Fitting the experiments allows to extract the random distribution of T_c at various carrier densities (or V_g). A similar approach is also adopted to fit the micrometrically averaged superfluid density in LAO/STO [9]. Assuming an effective two-band model with superconductivity triggered by the presence of few high-mobility carriers in a higher band, we account for the density dependence of the intra-puddle T_c within a simple BCS weak coupling scheme. As an important by-product we find that the range of variation in V_g of the (average) intra-puddle T_c is directly related (via μ) to the typical energy of the pairing mediator ω_0 .

S.C. and M.G. acknowledge financial support from “University Research Project” of the “Sapienza” University n. C26A115HTN. This work has been supported by the Region Ile-de-France in the framework of CNano IdF and Sesame programs, and by the DGA PhD program. Research in India was funded by the Department of Information Technology, Government of India.

-
- [1] N. Reyren, S. Thiel, A. D. Caviglia, L. Fitting Kourkoutis, G. Hammerl, C. Richter, C. W. Schneider, T. Kopp, A.-S. Retschi, D. Jaccard, M. Gabay, D. A. Muller, J.-M. Triscone, and J. Mannhart, *Science* **317**, 1196 (2007).
 - [2] A. D. Caviglia, *et al.*, *Nature (London)* **456**, 624 (2008).
 - [3] J. Biscaras, N. Bergeal, A. Kushwaha, T. Wolf, A. Rastogi, R. C. Budhani, and J. Lesueur, *Nat. Commun.*, **1**, 89 (2010).
 - [4] J. Biscaras, N. Bergeal, S. Hurand, C. Grossetete, A. Rastogi, R. C. Budhani, D. LeBoeuf, C. Proust, J. Lesueur, *Phys. Rev. Lett.* **108**, 247004 (2012)
 - [5] J. Biscaras, N. Bergeal, S. Hurand, C. Feuillet-Palma, A. Rastogi, R. C. Budhani, M. Grilli, S. Caprara, and J. Lesueur, arXiv:1209.6464 and *Nat. Mat.* (to be published).
 - [6] Ariando, X. Wang, G. Baskaran, Z. Q. Liu, J. Huijben, J. B. Yi, A. Annadi, A. Roy Barman, A. Rusydi, S. Dhar, Y. P. Feng, J. Ding, H. Hilgenkamp, and T. Venkatesan, *Nat. Commun.*, DOI: 10.1038/ncomms1192.
 - [7] J. A. Bert, B. Kalisky, C. Bell, M. Kim, Y. Hikita, H. Y. Hwang, and K. A. Moler, *Nat. Phys.* **7**, 767 (2011).
 - [8] Lu Li, C. Richter, J. Mannhart, and R. C. Ashoori, *Nat. Phys.* **7**, 762 (2011)
 - [9] Julie A. Bert, Katja C. Nowack, Beena Kalisky, Hilary Noad, John R. Kirtley, Chris Bell, Hiroki K. Sato, Masayuki Hosoda, Yasayuki Hikita, Harold Y. Hwang, Kathryn A. Moler, *Phys. Rev. B* **86**, 060503(R) (2012).
 - [10] A. D. Caviglia, M. Gabay, S. Gariglio, N. Reyren, C. Cancellieri, and J.-M. Triscone, *Phys. Rev. Lett.* **104**, 126803 (2010).
 - [11] S. Caprara, F. Peronaci, and M. Grilli, *Phys. Rev. Lett.* **109**, 196401 (2012).
 - [12] C. Bell, S. Harashima, Y. Kozuka, M. Kim, B. G. Kim, Y. Hikita, and H. Y. Hwang, *Phys. Rev. Lett.* **103**, 226802 (2009).
 - [13] B. Kalisky, private communication and APS March Meeting 2013.
 - [14] S. Ilani, private communication.
 - [15] S. Caprara, M. Grilli, L. Benfatto, and C. Castellani, *Phys. Rev. B* **84**, 014514 (2011).
 - [16] D. Stauffer and A. Aharony, *Introduction to Percolation Theory*, 2nd ed. (Taylor and Francis, London, 1994).
 - [17] Recent experiments [5] show evidence of inhomogeneities substantially smaller than a micron in LTO/STO, thereby supporting the present assumption of similarly small puddles in LAO/STO.
 - [18] D. Bucheli, S. Caprara, C. Castellani, and M. Grilli, *New J. Phys.* **15**, 023014 (2013).
 - [19] We point out that here and in Ref. 18 the fractal character (of the Diffusion Limited Aggregation type) of the generated

clusters has no intentional physical meaning, but is merely a technical artifice to generate dense, and yet filamentary, spatially correlated structures needed to reproduce tailish behavior of the the sheet resistance curves of oxide interfaces.

- [20] We checked that "bulky" inhomogeneities alone (i.e. without a long-distance filamentary structure) fail to reproduce the tailish resistance (see also Supplemental Material). Therefore the filamentary character with poor long-distance connectivity seems to be an essentially mandatory feature to reproduce the low-temperature behavior of $R(T)$.
- [21] D. Rakhmilevitch, I. Neder, M. Ben Shalom, A. Tsukernik, M. Karpovski, Y. Dagan, and A. Palevski, arXiv:1301.1055v1.
- [22] M. Salluzzo, J. C. Cezar, N. B. Brookes, V. Bisogni, G. M. De Luca, C. Richter, S. Thiel, J. Mannhart, M. Huijben, A. Brinkman, G. Rijnders, and G. Ghiringhelli, Phys. Rev. Lett. **102**, 166804 (2009).
- [23] Arjun Joshua, S. Pecker, J. Ruhman, E. Altman and S. Ilani, arXiv:1110.2184.
- [24] P. Delugas, A. Filippetti, V. Fiorentini, D. I. Bilc, D. Fontaine, and P. Ghosez, Phys. Rev. Lett. **106**, 166807 (2011)
- [25] Zhicheng Zhong, Anna Töth, and Karsten Held, arXiv:1209.4705v2.
- [26] R. M. Fernandes, J. T. Haraldsen, P. Wölfle, and A. V. Balatsky, Phys. Rev. B **87**, 014510 (2013)
- [27] C. S. Koonce, M. L. Cohen, J. F. Schooley, W. R. Hosler, and E. R. Pfeiffer, Phys. Rev. **163**, 380 (1967).

Supplemental Material for Inhomogeneity and multiband superconductivity at the $\text{LaTiO}_3/\text{SrTiO}_3$ and $\text{LaAlO}_3/\text{SrTiO}_3$ interfaces

In this supplemental material we provide further detail about the following two aspects of our work: the random resistor network used to model the inhomogeneous character of the oxide interfaces and to fit the experimental resistivity curves (section A) and the two-band model used to describe superconductivity inside the superconducting (SC) puddles (section B).

A. Details on the Christmas-tree model

To describe the inhomogeneous electric conductivity of $\text{LaTiO}_3/\text{SrTiO}_3$ and $\text{LaAlO}_3/\text{SrTiO}_3$ interfaces, we solve a random resistor network (RRN) consisting of two types of bonds: (i) normal bonds with a constant finite resistance $R_0 = 1$ and (ii) SC bonds with a temperature-dependent resistance $R^i = R_0 \theta(T - T_c^i)$, where T_c^i is the critical temperature of bond i and $\theta(x)$ is the Heaviside step function. The critical temperatures are random variables obeying a Gaussian distribution. The SC bonds form a spatially correlated cluster generated through a growth process known as *diffusion limited aggregation* (DLA) on which patches of circular shape with a diameter about 30 bonds long are superimposed, leading to a structure as shown in figure 7 (for details on the cluster growth see Ref. 18). The number of patches is chosen to yield RNNs with fractions of SC to total bonds equal to $w = 0.3, 0.4, 0.45, 0.5, 0.55, 0.6, 0.65, 0.7$.

Solving numerically Ohm's law on the bonds and Kirchoff's law for current conservation at the nodes of the network, the resistivity curves $R_w(T)$ are obtained. For a better statistic, we calculate $R_w(T)$ for 5 different realizations for each weight w and take the arithmetic average. These curves are then used to fit the experimental curves R_V measured at voltages $V = 50, 70, 100, 150, 200$ [V] in the following way: The high-temperature sheet resistance of the numerical solution is rescaled to the experimental one, with the exception of 100[V], 150[V] and 200[V], where, to avoid the high temperature step, the fit is only done for the temperature interval $[0.03, 0.21]$ and the sheet resistance is rescaled to $R_V(T = 0.21)$. The numerical temperature is then redefined to $\tilde{T} = (T - a)/b$, where a and b are chosen so as to minimize the difference

$$d = \sum_{T_j} |R_V(T_j) - R_w(T_j)|, \quad (3)$$

the sum running over all measured temperatures. The rescaled curve which minimizes the difference d , $R_{w=\bar{w}}(\tilde{T})$, is taken as the "correct" one and the sample at the corresponding voltage is assumed to have a weight of SC bonds equal to \bar{w} .

In addition to the quasi 1D long-range connectivity and quasi 2D short-range connectivity, the Christmas-tree model has the characteristic of closed loops covering almost entirely the cluster. With the size of a bond about 10 nm , these loops are of the order of a micrometer. This aspect is relevant when interpreting superfluid density measurements. Indeed, the question arises about the magnetic response measured when performing a SQUID experiment, the SQUID pick-up coil recording the local magnetic field produced by a field coil that extends over a few micrometers. Under these conditions, the measurement resolution exceeds the (average) size of a loop and the measurement cannot distinguish whether a closed loop encompasses a SC or a non-SC region. More precisely, the SC loops being smaller than the experimental resolution, the SQUID sees all bonds inside a loop as if they were SC. As a result, the SQUID experiment can yield a superfluid fraction $w \sim 1$ all the while the transport measurements yield resistivity curves that can be fitted with $\bar{w} \sim 0.5$.

While fitting the experimental data may seem to require simply a cluster with a small long-range connectivity and a high density, we stress that the issue is more subtle than that. Indeed, we considered a series of clusters sharing some characteristics of the Christmas-tree model and calculated the corresponding resistivity curves (see figure 8). Starting from the assumption that the cluster should be filamentary, dense and possibly exhibit loops, we considered a symmetric random walk (SRW) as shown in figure 4. Even though the connectivity is rather small, it is too large to yield pronounced tails as experimentally observed. In order to make the system more 1D and possibly denser, we reduced the number of random walks and superimposed SC patches (obtaining a cluster similar to the Christmas-tree) as shown in figure 5. One does obtain a tailish feature at low temperature, which however is not in agreement with the experimental data. Moving on to a DLA cluster without patches (figure 6), we found resistivity curves leading to rather satisfactory fits of the transport data. However, this cluster does not exhibit loops and, as a theoretical drawback, one cannot easily tune the density with keeping the long-range connectivity low. Finally, when adding

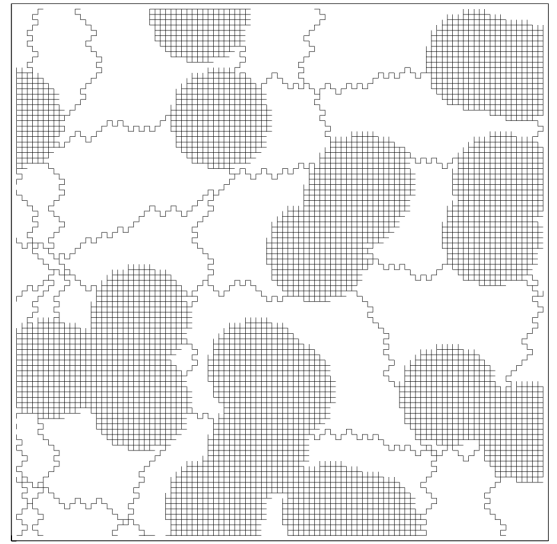
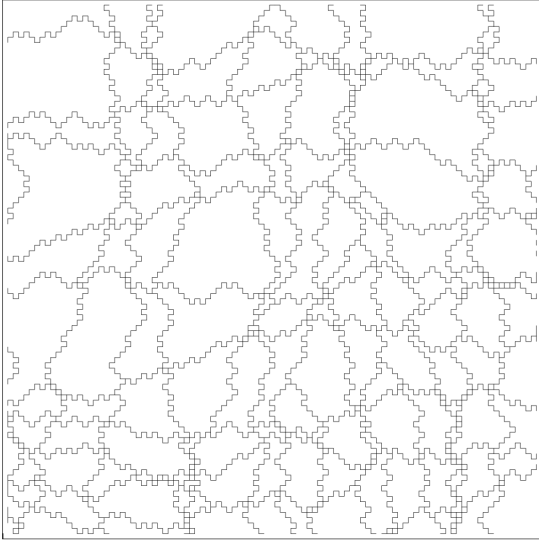


FIG. 4. Symmetrized random walk cluster without patches;FIG. 5. Symmetrized random walk cluster with patches; weight $w = 0.2$. $w = 0.5$.

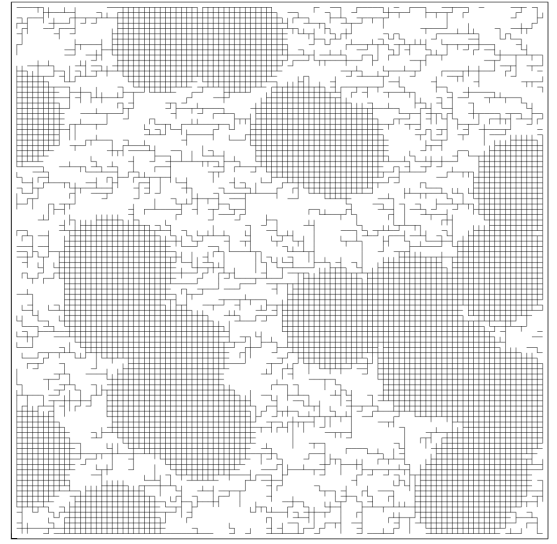
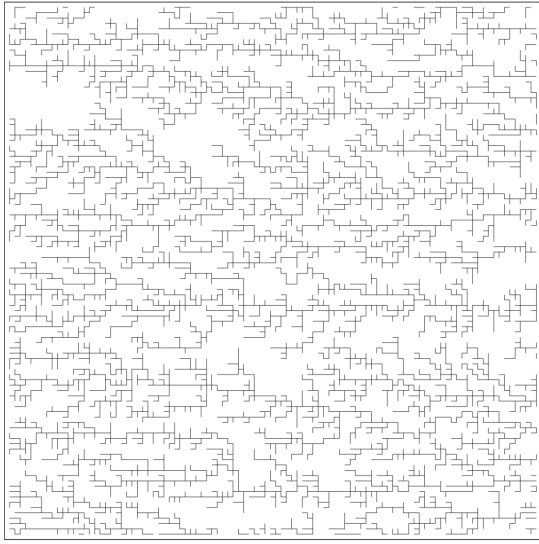


FIG. 6. Diffusion limited aggregation cluster without patches;FIG. 7. Diffusion limited aggregation cluster with patches; weight $w \approx 0.3$. $w = 0.6$.

patches, these two limitations are overcome, which leads us to conclude that our Christmas-tree model captures the main features of the SC state at the interface.

B. Two-band superconductivity for LXO/STO interfaces

We propose that the 2DEG formed at the LTO/STO interface may be described as a multiband system, and the occurrence of superconductivity may be captured by means of a BCS-like Hamiltonian

$$\begin{aligned} \mathcal{H} = & \sum_{\mathbf{k}, \ell} \sum_{\sigma=\uparrow, \downarrow} (\varepsilon_{\mathbf{k}, \ell} - \mu) c_{\mathbf{k}, \ell, \sigma}^\dagger c_{\mathbf{k}, \ell, \sigma} \\ & + \frac{1}{N} \sum_{\substack{\mathbf{k}, \mathbf{k}' \\ \ell, \ell'}} \widetilde{g_{\ell \ell'}} c_{\mathbf{k}, \ell, \uparrow}^\dagger c_{-\mathbf{k}, \ell, \downarrow}^\dagger c_{-\mathbf{k}', \ell', \downarrow} c_{\mathbf{k}', \ell', \uparrow} \end{aligned} \quad (4)$$

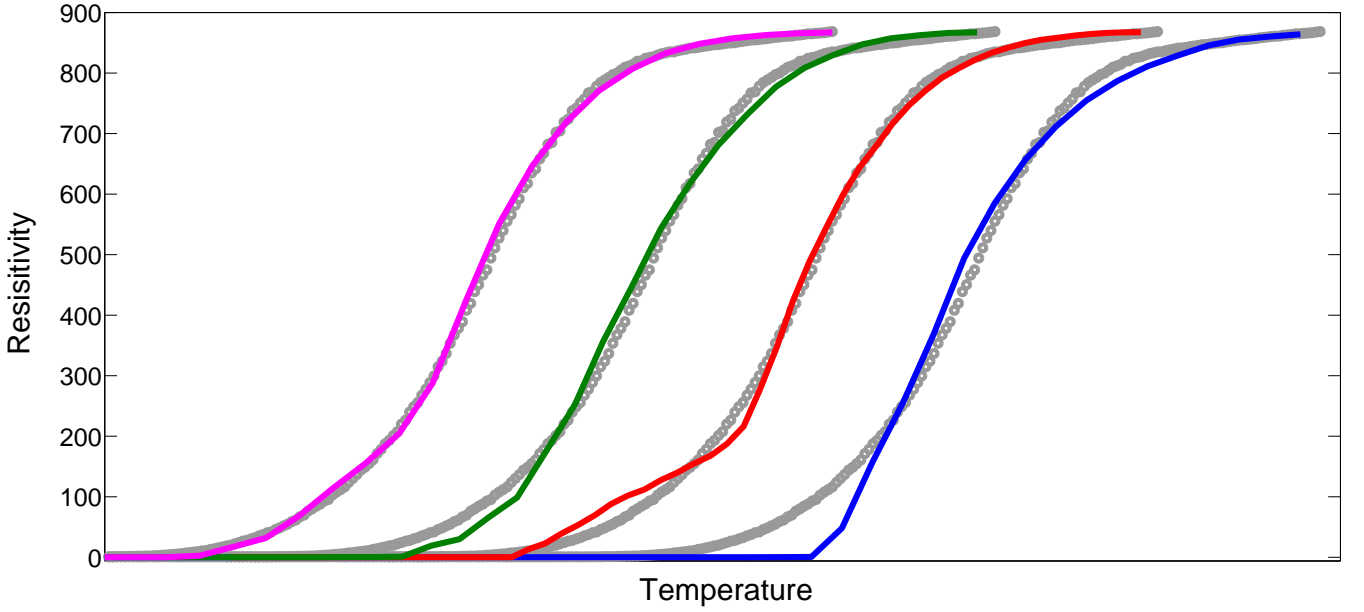


FIG. 8. Fit of resistivity curve measured at $V = 100$ [V]. Grey curves report the experimental data $R_{V=100}$ (duplicated and shifted for ease of reading), coloured curves report (from left to right) numerical calculations obtained for DLA with patches, DLA without patches, SRW with patches, SRW without patches.

where $c_{\mathbf{k},\ell,\sigma}^\dagger$ ($c_{\mathbf{k},\ell,\sigma}$) creates (annihilates) an electron with two-dimensional wave vector \mathbf{k} , parallel to the plane of the interface, and spin projection σ , belonging to the ℓ -th sub-band, with dispersion law

$$\varepsilon_{\mathbf{k},\ell} = \bar{\varepsilon}_\ell + \frac{\hbar^2 k_x^2}{2m_{\ell,x}} + \frac{\hbar^2 k_y^2}{2m_{\ell,y}}.$$

Hereafter, $\bar{\varepsilon}_\ell$ label the levels arising both from the level quantization inside the confining potential well and from the various bands mostly due to the t_{2g} orbitals of Ti in STO. m is the (possibly anisotropic) effective mass of the 2D charge carriers, μ is the chemical potential, N is the number of \mathbf{k} vectors allowed by the boundary conditions in the first Brillouin zone of the two-dimensional lattice. The parameters $g_{\ell\ell'}$ are the (intraband for $\ell = \ell'$, interband for $\ell \neq \ell'$) pairing amplitudes, and the tilde in Eq. (4) indicates that the sums are restricted to electron states such that $|\varepsilon_{\mathbf{k},\ell} - \mu|, |\varepsilon_{\mathbf{k}',\ell'} - \mu| \leq \hbar\omega_0$, where ω_0 is a characteristic frequency of the mode that mediates pairing.

In our description of the LTO/STO interface, we assume, for simplicity, that only two sub-bands, labeled by $\ell = 1, 2$, are involved. The $\ell = 1$ sub-band contains the low-mobility carriers found in Refs. 4 and 12, whereas the $\ell = 2$ sub-band accommodates the high-mobility carriers. The SC puddles are regions where the sub-band $\ell = 2$ is locally filled, whereas the metallic (or weakly localized) background corresponds to regions where the sub-band $\ell = 2$ is empty. To reproduce the experimental results, we are led to assume that $g_{11} \ll g_{12}, g_{21} \ll g_{22}$ (this condition is consistent with the analysis of two-band model in Ref. 26, but different assumptions $g_{11} \lesssim g_{12}, g_{21}$ or $g_{12}, g_{21} \lesssim g_{22}$, would lead to similar conclusions as far as the present analysis is concerned). Finite g_{12}, g_{21} guarantee that superconductivity is induced in the first sub-band, as soon as it establishes in the second sub-band.

The equation that determines the SC critical temperature T_c in a two-band system is

$$[1 - g_{11}\Pi_1(T_c)][1 - g_{22}\Pi_2(T_c)] = g_{12}g_{21}\Pi_1(T_c)\Pi_2(T_c)$$

where

$$\Pi_\ell(T) = \int_{|z| < \beta\hbar\omega_0} \frac{dz}{2z} N_\ell(z) \tanh\left(\frac{z}{2}\right),$$

$\beta = (\kappa_B T)^{-1}$, $N_\ell(z) = N_\ell^0 \vartheta(z - \beta\bar{\varepsilon}_\ell + \beta\mu)$ is the density of states of the ℓ -th sub-band (in the dimensionless variable $z = \beta\varepsilon$), with $N_\ell^0 = a^2 \sqrt{m_{\ell,x} m_{\ell,y}} / (2\pi\hbar^2)$, a being the spacing of the two-dimensional lattice. There are four possible regimes for $\Pi_\ell(T)$: if $\bar{\varepsilon}_\ell - \mu > \hbar\omega_0$, the chemical potential falls below the bottom of the band and there are no states available for pairing within the shell of width $2\hbar\omega_0$, hence $\Pi_\ell(T) = 0$; if $0 < \bar{\varepsilon}_\ell - \mu < \hbar\omega_0$, the chemical potential still

falls below the bottom of the band, but there are some states available for pairing within the shell of width $2\hbar\omega_0$, hence $\Pi_\ell(T) = N_\ell^0 \ln[\sqrt{\hbar\omega_0}/(\bar{\varepsilon}_\ell - \mu)]$; if $-\hbar\omega_0 < \bar{\varepsilon}_\ell - \mu < 0$, the chemical potential falls within the band, although there are some states unavailable for pairing within the shell of width $2\hbar\omega_0$, hence $\Pi_\ell(T) = N_\ell^0 \ln[1.14 \beta \sqrt{(\mu - \bar{\varepsilon}_\ell)\hbar\omega_0}]$; if $\bar{\varepsilon}_\ell - \mu < -\hbar\omega_0$, the chemical potential falls within the band and all the states within the shell of width $2\hbar\omega_0$ are available for pairing. In this case the standard BCS result $\Pi_\ell(T) = N_\ell^0 \ln(1.14 \beta \hbar\omega_0)$ is recovered. We do not report here the crossover expressions when $|\bar{\varepsilon}_\ell - \mu| \lesssim \kappa_B T$; we also assumed that $\hbar\omega_0 \gg \kappa_B T$, since we shall show that our system is indeed in the weak-coupling regime (i.e., $N_\ell^0 g_{\ell\ell'} \ll 1$ for all the coupling constants $g_{\ell\ell'}$).

We assume henceforth that the bottoms of the two sub-bands are well separated, $\bar{\varepsilon}_2 - \bar{\varepsilon}_1 \gg \hbar\omega_0$, and take $\bar{\varepsilon}_2 = 0$ as the reference energy level. For $g_{11} = 0$, the system is not SC until the filling reaches the value such that $\mu = -\hbar\omega_0$. However, T_c will stay exponentially small, until $\mu = 0$. In particular, letting $\mu \equiv -\hbar\omega_0 + \delta\mu$, for $\delta\mu \rightarrow 0^+$ we find

$$T_c \approx 1.14 \hbar\omega_0 e^{-2\hbar\omega_0/(N_1^0 N_2^0 g_{12} g_{21} \delta\mu)}.$$

In the following, we assume that $T_c = 0$ in this regime. In the range $0 < \mu < \hbar\omega_0$, T_c becomes sizable and increases with increasing μ . Neglecting small corrections due to g_{12} and g_{21} one finds

$$T_c \approx 1.14 \sqrt{\hbar\omega_0 \mu} e^{-1/(N_2^0 g_{22})}, \quad (5)$$

while, for $\mu > \hbar\omega_0$, T_c saturates to its maximum (BCS) value

$$T_c^{max} \approx 1.14 \hbar\omega_0 e^{-1/(N_2^0 g_{22})}. \quad (6)$$

Thus, $T_c(\mu) = 0$, for $\mu < 0$, $T_c(\mu) = T_c^{max} \sqrt{\mu/\hbar\omega_0}$, for $0 \leq \mu \leq \hbar\omega_0$, $T_c(\mu) = T_c^{max}$, for $\mu \geq \hbar\omega_0$, and the range of variation of μ which corresponds to an increasing T_c is a direct measure of the characteristic energy scale of the pairing mediator, $\hbar\omega_0$.

The chemical potential μ is related to the variation of the carrier density δn in the second sub-band as $\mu = \delta n/(2N_2^0)$. On the other hand, we extract the value of $\delta n(V_g)$ from a self-consistent calculation of the sub-band structure in the quantum confining potential [4], in the presence of the gate voltage V_g . The procedure is the following: for each V_g the full numerical solution of the coupled Schrödinger and Poisson equations yields the sub-band structure in the confining potential; the Fermi level E_F is then fixed to accommodate all the carriers; the SC sub-band is identified as the one that starts to be filled in correspondence of the value of V_g at which superconductivity is observed to occur; the chemical potential μ entering in our two band model is obtained as the difference between E_F and the bottom of the SC sub-band.

We are thus able to extract the dependence $\mu(V_g)$ to describe the chemical potential entering the $\ell = 2$ band of the SC carriers and obtain the fit to the experimental data shown in Fig. 3, for the set of parameters considered in Ref. [4], where the sub-bands have all d_{xy} character, with light isotropic mass $m_{x,y} \approx 0.7 m_0$.